Journal of Applied Electrochemistry **30**: 899–913, 2000.

Hydrodynamic modelling of direct methanol liquid feed fuel cell stacks

P. ARGYROPOULOS, K. SCOTT and W.M. TAAMA
Chemical and Process Engineering Department, University of Newcastle upon Tyne, Merz Court, Newcastle upon Tyne, NE1 7RU, Great Britain

Received 13 April 1999; accepted in revised form 1 February 2000

Key words: direct methanol fuel cell, DMFC stacks, manifold distribution, modelling, pressure drop

Abstract

A model for the liquid feed, direct methanol fuel cell (DMFC), based on the homogeneous two-phase flow theory and mass conservation equation, which describes the hydraulic behaviour of internally manifolded cell stacks, is presented. The model predicts the pressure drop behaviour of the anode side of an individual DMFC cell and is used to determine the channel depth and width for fast and efficient carbon dioxide removal with minimum pressure drop. The model is used to calculate flow distribution through fuel cell stack internal manifolds. The effect of inlet and outlet manifold diameters on flow distribution is also determined. Two types of manifold design are compared, reverse flow and parallel flow. An iterative numerical scheme is used to solve the differential equations for longitudinal momentum and continuity.

List of symbols

d	diameter (m)
f	friction factor
G	mass velocity (kg m^{-2} s^{-1})
g	standard gravitational acceleration (ms^{-2})
k	hydraulic resistance
l	length (m)
L	manifold length
n	number of electrons transferred through the cell
ncs	number of stacked cells
Δp	pressure drop
Q	volumetric flow rate (m^3 s^{-1})
q	cell volumetric inlet flow rate (m^3 s^{-1})
Re	Reynolds number
x_o	mass fraction of the dispersed phase
u	velocity (m s^{-1})
x	manifold dimension
y	step length (m)

Subscripts

cor	corrected
d	depth
f	liquid
fb	flow bed
fg	(liquid–gas)
g	gas
gf	(gas–liquid)
h	hydraulic
inlet	inlet condition
k	iteration number
H	header
w	width

Greek letters

α	area (m^2)
μ	viscosity (kg m^{-1} s^{-1})
ρ	density (kg m^{-3})
ó	variance
v	specific volume (kg m^{-3})
χ	electroosmotic drag coefficient

1. Introduction

Direct methanol fuel cells (DMFC), using solid polymer electrolyte (SPE) membranes (e.g., Nafion®), are considered to be promising power sources, especially for vehicular applications. This fuel cell has many important attributes; quick refuelling, low temperature and pressure operation, low fuel cost, possible use of existing fuel distribution infrastructure, no liquid electrolyte and compact cell design. The main drawbacks of the cell to date are; methanol crossover through the membrane, with the production of a mixed potential at the cathode and a loss of fuel efficiency, and the lack of a highly active, cheap and efficient electrocatalyst [1, 2].

Direct methanol fuel cell (DMFC) stacks are under development at a number of research groups world-wide

[1, 3–14]. There are a number of scientific and technological issues yet to be solved with the DMFC, and most concern the electrochemical problems associated with methanol oxidation, crossover etc., where the research effort has focused on improving the electrochemical performance of these cells [15–19]. However there are also important engineering design aspects that remain to be studied, that have been mainly neglected.

Recently, we have developed engineering models concerning DMFC stack thermal management and overall system pressure drop [20–24]. The models help the understanding of the processes that occur inside a DMFC system, their interactions, and the overall system behaviour. This then enables assessment of auxiliary equipment requirements to operate the fuel cell stack, which also has some bearing on the actual electrochemical performance of the fuel cell. The features of the model relate to the influence of methanol crossover, the generation of carbon dioxide gas, the vaporisation of methanol, and of water, from the cell streams and the hydraulic connection of cells in a large-scale stack. A sound knowledge and understanding of how the operating and systematic parameters affect the cell behaviour will be a valuable source of information on deciding the system characteristics.

This paper is divided in two parts. The first uses the previously developed model for single cell pressure drop behaviour [20, 21], which is used to investigate the effect of flow channel dimensions on the pressure drop behaviour in the anode side of the cell. In the second part another model, which predicts the flow distribution in the cells of a DMFC stack [24] is used to compare the flow distributions obtained with two types of internal flow manifolds, parallel flow or reverse flow. Overall the present study presents a methodology for the evaluation of different stack designs and configurations, and, although it is applied for the specific stack system design developed in Newcastle, it can be used for other stack designs with modifications to the geometric details of the cells.

2. Mathematical modelling of a DMFC stack

One of the aspects in the stacking of fuel cells is how well the reactants are distributed along a stack consisting of a large number of fuel cells. If fluids are not evenly distributed we can have localised feed or oxidant starvation, which will lower the cell performance. In addition this could lead in localised carbon dioxide accumulation, in the case of the DMFC, which can cause instabilities in both short term and long-term operation. The main parameters, which affect the flow distribution inside the cell stack, are the reactant flow rates and the hydraulic resistances that reactants experience flowing through the system. These resistances are: (i) that caused by the flow through the manifold channels, the manifold channels can be regarded as pipes with rough surface; (ii) that result from the splitting of the flow in the inlet manifold channels; (iii) that result from the combining of the flow in the outlet manifold channels; and (iv) that caused from the two-phase flow conditions prevailing in the larger portion of anode and cathode side total flow length.

To achieve a constant and steady operation it is necessary to avoid, or minimize, all type of flow maldistribution.

2.1. *Flow maldistributions*

In the present model of the flow distribution in electrochemical cell manifolds, the analysis used in plate and frame heat exchangers is used, with suitable modifications, which allow for the phenomena that occur in electrochemical cells; that is, carbon dioxide evolution, reactants consumption, and transition between single phase and two phase flow conditions.

There are essentially three types of possible flow maldistribution: within the channel, channel to channel and manifold induced. Within the channel flow maldistribution occurs, in those cases when there is a nonuniform flow distribution in the plate bed design. Extensive flow visualisation studies conducted in our laboratory proved that the fuel cell flow bed design [41], shown in Figure 1(a), achieves a uniform flow distribution.

Channel-to-channel flow maldistribution occurs in stacks, which have a different plate design geometry in each side. In our case the plate design is identical and hence this type of flow maldistribution is ignored.

Manifold induced flow maldistribution occurs as inlet and outlet ports, on a given fluid side in a plate stack, form inlet and outlet manifolds to distribute the fluid in and out of the stack. Different fluid streams, both in composition and throughput, flowing through inlet manifold, plate passages and outlet manifold experience different total flow lengths. Since each fluid stream must experience the same total pressure drop (the difference between inlet and outlet pressures), while flowing through different flow lengths, this can result in flow maldistribution. This effect generally becomes more severe as the number of plates per pass is increased and also in the case of highly viscous liquids being cooled.

2.2. *Manifold flow distribution characteristics*

Lateral flow is defined here as the flow through a branch of the manifold (i.e. a stacked cell). The lateral flow for a branch of a manifold is primarily determined by the pressure difference between the entrance and the exit of the lateral path and the reaction-taking place inside the cell. Three factors affect the pressure in a manifold header and therefore determine flow through lateral paths: (i) pressure drop due to frictional losses; (ii) pressure recovery; and (iii) pressure drop due to the change in flow bed geometry or system volume. For example, for a dividing flow manifold (i.e., a manifold that distributes a fluid through multiple openings), frictional losses cause the pressure to drop through the manifold header, while removing fluid through the lat-

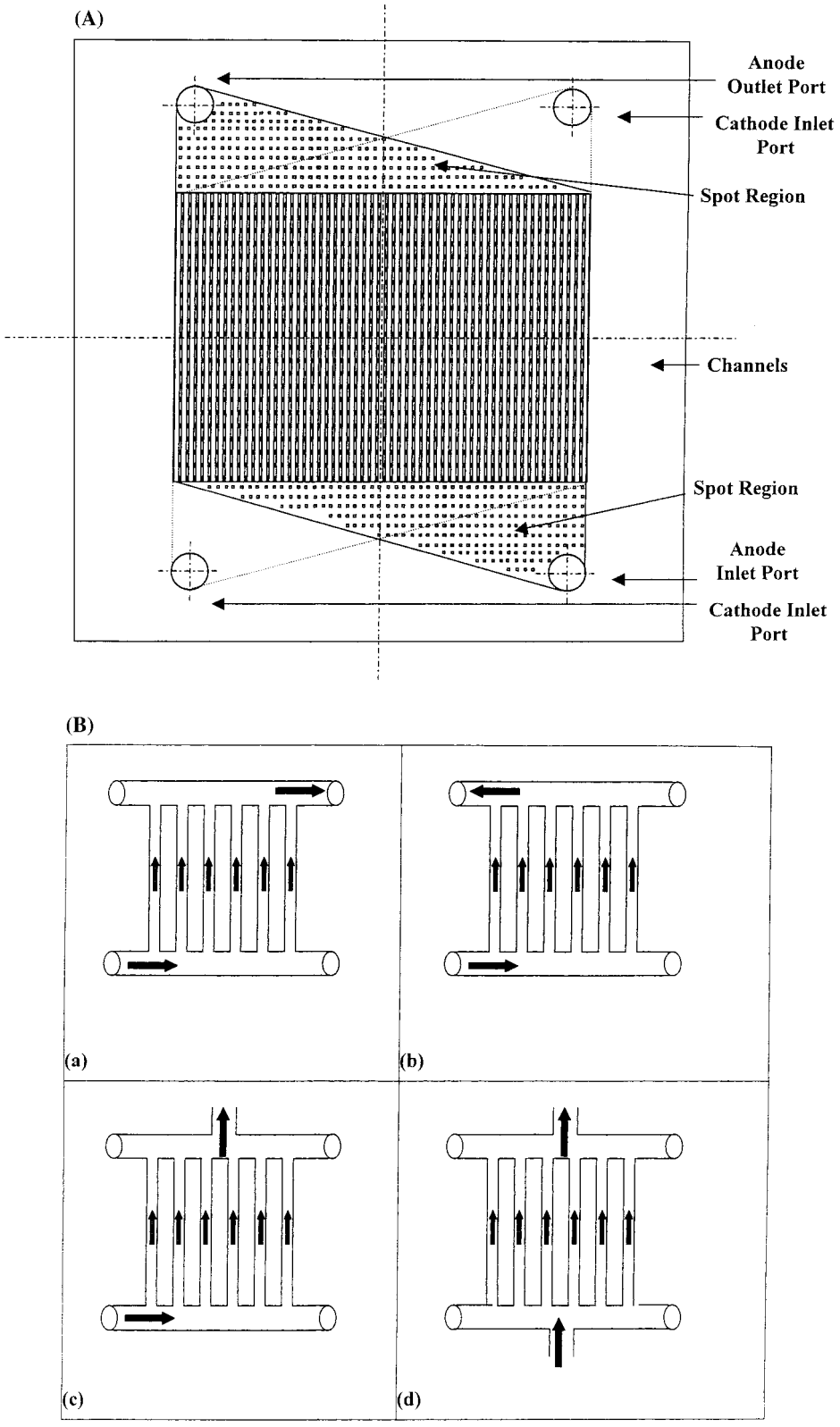

Fig. 1. (A) Flow bed design. (B) Schematic representation of parallel (a), reverse (b), and mixed flow manifold configuration (c, d).

eral paths causes the pressure to increase down the manifold header [25].

There are two important factors that determine the distribution of flow in and out of manifolds: (i) inertia or, more exactly, the momentum of the main fluid stream flowing into a manifold tends to carry the fluid toward the closed end, where an excess pressure is produced; and (ii) friction of the fluid against the internal surface of the main channel reduces the pressure in the direction of flow.

On the one hand, (i), corresponds to change of velocity head. In general, as the fluid flows along the

manifold its longitudinal velocity decreases, due to part of the fluid volume being discharged laterally through the openings. Therefore, the fluid flow in the manifold is decreased and, in accordance with Bernoulli's theorem, this increases the fluid pressure. Friction, (ii), on the other hand, results in loss of pressure along the length. The relative magnitudes of the pressure regain due to deceleration and the pressure loss due to friction determine whether the pressure rises or falls from the inlet end to the closed or dead end of the manifold.

When the fluid flows into the manifold and undergoes subdivision, that is, a 'blowing manifold' the friction and momentum effects work in opposite directions, the first tending to produce a pressure drop and the second an increase in pressure. When the stream is formed in the manifold by the combination of smaller streams and flows from the open end of the main channel, that is, a 'sucking manifold' the friction and momentum effects reinforce each other, creating lower pressures at the open end than at the closed end [26, 27].

The flow field in the header of manifold systems can be regarded as one dimensional, for many practical purposes. However, due to the elliptic nature of the flow in the header, the Bernoulli equation cannot be applied. The difficulty with applying a Bernoulli equation to the branching process lies in the ambiguity, which exists in identifying a relevant streamline on which to conserve energy and estimate frictional losses [28, 29]. On the other hand, it is necessary to solve simultaneously the longitudinal momentum equation, the continuity equation in the header, and the discharge equation in the lateral branches to obtain the static pressure and the two components of velocity. Most of the manifold flow distribution models available in the open literature were developed for the case of steam generators (e.g., [25, 30]). Subsequently they were based on the fact that the mass was conserved in the whole system and simply changed phase (from liquid to gas or vice versa). Unfortunately this type of analysis is not applicable to the DMFC stack, which is an electrochemical system with reactions taking place in its interior. Mass is consumed/produced from reactions, and in addition water [31–33] and methanol [16, 17, 34] are transferred through the membrane, from the anode to the cathode side, due to the electroosmotic drag. Hence none of the aforementioned models are suitable for the DMFC stack. Boersma [35] recently presented a model for gas distribution in fuel cell stacks but their lack of information on flow bed design limited their ability to solve explicitly their model. Our model, which is presented below, takes under consideration some aspects of that model.

2.3. *Basic manifold distribution model equations*

In a DMFC stack the manifolds have a circular cross section and the channels are rectangular. The flow is laminar, with very low Reynolds number, for the rectangular channels of the graphite bipolar plate, while, in the case of circular manifolds, the flow can be either laminar or turbulent depending on the total flow rate in both sides of the cells. The analysis is complicated by the fact that in a DMFC environment there is two-phase flow at the anode side where carbon dioxide bubbles flow with the methanol solution inside the channels, and larger gas pockets are present inside the anode side outlet manifold. Often, depending on the actual operating temperature, the water and methanol are partly in vapour form (in the case of elevated temperatures and pressures), while at medium temperatures they are both in liquid form.

Before proceeding with the analysis a few comments should be made concerning the hydrodynamic conditions for fully developed flow. According to Incropera [44], for laminar flow, the required flow length to reach fully developed flow is given by an equation of the form:

$$\frac{l_{\mathrm{f,req}}}{d_{\mathrm{tube}}} \approx 0.05\,Re \tag{1}$$

where l is the required tube length in metres and d is the tube diameter.

For the case of turbulent flow there is no general satisfactory expression for the entry length but, in general, it is accepted that this length is independent of the Reynolds number and, as a first approximation, can be calculated from an expression of the form:

$$10 \leqslant \frac{l_{l,\mathrm{req}}}{d_{\mathrm{tube}}} \leqslant 60 \tag{2}$$

Nevertheless, for simplicity, it is assumed that fully developed turbulent flow takes place for $(l/d) > 10$ [44].

Simple calculation of the required lengths to reach such conditions show that these lengths are restricted to a few centimetres close to the inlet and outlet ports. As these lengths are much shorter than the length of, for example, the flow bed, the assumption of fully developed flow is adopted.

The pressure drop, Δp, inside a part of the circular cross section manifold can be calculated from the following equation:

$$\Delta p = \frac{1}{2}\left(\rho u^2 \frac{l(f+k)}{d_{\mathrm{h}}}\right) \tag{3}$$

where d_{h} is the hydraulic diameter, u the flow velocity, l is the pipe length, ρ is the fluid density, f is the hydraulic resistance coefficient which is strongly dependent upon Reynolds number, and k is the hydraulic resistance due to flow splitting or combining. The hydraulic resistance k is fully dependent on the ratio of flow rate supplied to each cell divided by the remaining flow rate, after the split, for the case of 'flow splitting', and similarly for other case. Data for these coefficients is tabulated by Beitz [36], or can be found in a graphical form in VDI Warme–Atlas [37]. In the view of many other uncertainties with two-phase flow correlations, the friction factors are adequately represented as [38]:

$$f = \begin{cases} \dfrac{64}{Re} & \text{for } Re < 2000 \text{ (Poiseuille equation)} \\ \dfrac{0.32}{Re^{0.25}} & \text{for } Re > 2000 \text{ (Blasius equation)} \end{cases} \tag{4}$$

The most critical part in a DMFC stack is the flow bed in each side (i.e., the flow pattern machined on either side of a bipolar plate and is responsible for reactants/product supply/removal to/from the cell). We have recently presented a model for the pressure drop characteristics of the anode and cathode side of a DMFC cell [20, 21]. The equation used for calculating the pressure drop for the anode side is:

$$\Delta p = \int_0^{l_1} \left\{ \begin{array}{c} \left[G^2(y) \left[\dfrac{2(yf(y)+K_1)v_f(y)}{d_{H,ge}} + (v_f(y) - v_{fg}(y)) \right] + \dfrac{gy}{v_{fg}(y)} \right] \\ G^2(y) \left[\dfrac{2(yf(y)+K_1)v_f(y)}{d_{H,ge}} \times \left(1 + \dfrac{x_0(y)v_{fg}(y)}{2v_f(y)} \right) + (v_f(y) - v_{fi}(y)) + v_{fg}(y)x_0(y) \right] \\ + \dfrac{gy}{v_{fg}(y)x_0(y)} \ln\left(1 + x_0(y) \dfrac{v_{fg}(y)}{v_f(y)} \right) \end{array} \right\} dy \tag{5}$$

The first part (in square brackets) of Equation 5 represents pressure drop for single-phase flow, that is, when there is no electrochemical activity (zero load) or when the maximum solubility (dependent on local temperature, pressure and mixture composition) of carbon dioxide in the aqueous methanol solution is not exceeded.

The second part (in square brackets) of the above equation has four terms: the first term denotes the frictional pressure drop for two-phase conditions; the second term accounts for the acceleration of the liquid due to a change in the specific volume which produces a small pressure drop; and the third term represents acceleration pressure drop for the two-phase flow. The third term of Equation 5 is for the two-phase gravitational head.

Equation 5 can be used to describe the single phase (inlet anode side manifold) and two phase flow conditions for the anode side outlet manifold.

The velocities at the two ends ($x = 0$ and $x = L$) of the manifolds are:

1. for the case of a reverse flow dividing manifold

$$x = 0, \quad u = u_{inlet} = \frac{Q_{inlet}}{\rho \alpha_H} \tag{6}$$

$$x = L, \quad u = 0 \tag{7}$$

2. for a combining manifold

$$x = 0, \quad u = u_{outlet} = \frac{Q_{outlet}}{\rho \alpha_H} \tag{8}$$

$$x = L, \quad u = 0 \tag{9}$$

The model predictions for the anode and cathode side flow beds of a single DMFC cell are extensively discussed in the relative publications [20, 21]. To aid the understanding of the model predictions presented here we briefly summarize the model predictions for the anode side of a DMFC. Altering the inlet temperature, the methanol concentration or the overall anode side temperature gradient has a small effect on the overall pressure losses. On the contrary, volumetric flow rate and current density have a more profound effect on pressure losses. In general increasing the flow rate increases the friction losses, while increasing current density reduces overall losses since it leads to the production of larger quantities of carbon dioxide gas. The model is based on the assumption that the anode liquid is fully saturated with carbon dioxide as in practice the feed is recycled from an external reservoir or from a gas liquid separator.

In its present form the model does not consider the vapour–liquid equilibrium between the water and methanol solution and the gaseous phase and the effect of these phenomena on the thermal management. These are the subject of detailed modelling currently being evaluated. The scope of this study is to establish a systematic theoretical procedure for designing a fuel cell stack. To accurately model the real flow situation inside a working DMFC environment it is essential to have exact information concerning the localized pressure and temperature, which are strongly dependent on the flow bed design, adopted. Hence, the use of the current mathematical model is focused on the geometrical details of the flow bed and manifolds in a range of values where an 'optimum' design is likely to exist in practice.

The experimental validation of the above model is extremely difficult. The nature of the system, particularly the compact nature of the cell stack and the very low flow bed depths (2 mm), make the insertion of a suitable flow measurement device near the cells inlet or outlet ports extremely difficult. However, measurements of a model device is of limited use since the exact stack conditions and, especially, the electrochemical activity cannot accurately be represented. For these reasons the present model is designed as a tool to provide predictions of real stack operation with an aim of optimising the stack geometry.

2.4. *Solution methodology*

To solve the flow distribution model, initially a uniform flow distribution is applied in all branches. The

pressure drop of the manifold is then initially calculated based on this assumption. With the flow rate in the inlet of the individual cells now estimated the cell pressure drop is calculated with the aid of the pressure drop model. That model is able to calculate the composition and the outlet volumetric flow rate. Then from these results we can calculate the pressure drop in the exhaust manifold. Theoretically the pressure drop in each branch should be equal with the adjacent ones, while typically, the pressure drops resulting from the first iteration are not. A correction procedure is then applied as follows. The average value and the standard deviation of all the branches pressure drops is calculated and also the variance of each branch. The total calculated pressure drop is divided by the anode side inlet liquid flow rate in order to correlate the pressure drop with the inlet flow rate. This gives a correction factor of pressure drop per unit liquid flow rate. Then the initial inlet guessed flow rates are corrected according to the formula:

$$q_{\mathrm{in,i,cor,p}} = q_{\mathrm{in,i}} + \left(\sigma \times \frac{Q_{\mathrm{in}}}{\sum_i \Delta p}\right) \tag{10}$$

where, σ, is the variance of the ith cell.

In general the predicted corrected flow rates are not compatible with continuity for the inlet manifold. Another correction is made to conform to that principle:

$$q_{\mathrm{in,i,cor,c}} = q_{\mathrm{in,i,cor,p}} + \left(\frac{Q_{\mathrm{in}} - \sum_i q_{\mathrm{in,i,cor,p}}}{ncs}\right) \tag{11}$$

Then with the corrected flow rates another iterative cycle starts. The convergence criterion is determined as

$$\sigma_{\mathrm{k}}^2 \leqslant 0.0001 \tag{12}$$

The physical meaning of such a criterion is that all the branch pressure drops will be in a very narrow range around the mean value and will differ by only a few Pa. The model converges after a few decades of iterations, and gives accuracy, within 5 Pa, for the pressure drops.

3. Results and discussion

The flow bed design used for the experimental stack studies at Newcastle (Figure 1) is based on a compact heat exchanger concept, and is divided into three sections: a triangular enlarging inlet section, 20 mm long, with a series of 2 mm^2 rectangular spots, a central flow bed consisting of 57 parallel channels of 4 mm^2 cross section and a triangular, outlet section, of a similar design to the inlet section. Methanol solution supply to the cell is at the bottom from a 15 mm diameter inlet at one corner of the graphite plate. Methanol solution and carbon dioxide gas leave at the opposite corner at the top of the cell from a 25 mm diameter port. The model considers this to be the basic design and varies geometric details of channel size and manifold size.

Although the generalization of the model with the use of dimensionless groups is highly desirable it is not an easy task due to several factors. The flow maldistribution identified as a problem in stacked cells means that the flow velocity can vary significantly within the stacked cells. The flow bed is based on a variable cross-section geometry, which further affects the magnitude of the fluid velocity related parameters. In particular the electrochemical activity of the system and the transition from single phase to two-phase flow conditions further complicates the comparison of the results. In general anode side inlet flow rate is a parameter that can be monitored easily and to some extent it can be linked with the total stack active area in order to be able to compare different stack systems. In this model system a typical methanol solution flow rate of 1 $dm^3\ min^{-1}$, with a channel dimension of 4 mm^2, is equivalent to a channel velocity of 7.3 cm $s^{-1}$and a Reynolds number of approximately 146. It will be apparent in the data generated by the model and discussed below that there is no generalised correlation possible due to the complexity of the system. Overall the present model is designed as a tool for system design and screening of various alternative designs and, with proper modifications in the model geometry, can be used generally for any internally manifolded stack system.

3.1. *Flow bed channel dimensions*

The bipolar plate flow beds in a DMFC are typically made from a thin non-porous graphite block (in the present case 8 mm). In general the design of the flow bed and its geometric details (like channel shape, width and depth) are determined semi-empirically, based on previous experience and on the material characteristics of the graphite. A design requirement for the bipolar plate is to be as thin as possible, to minimize the stack volume and the parasitic voltage loss. The flow channels in the plate should be closely spaced to provide support to the membrane electrode assembly and to provide efficient collection of the current from the carbon cloth surface of the MEA. However, machining graphite imposes practical limitations to the channel size. The influence of the rib spacing in hydrogen PEM fuel cell assemblies has been modelled to assess water and current distribution [39]. For the cases considered in that work the rib spacing only slightly alters the half-cell potential but has a significant influence on water management. In the case of the liquid feed DMFC the issue of water distribution in the anode side of the cell is not likely to be a major issue.

We have recently developed a two-phase flow model for calculating the pressure drop behaviour of the DMFC [20, 21]. The model was used to investigate the effect of the operating parameters (inlet flow rates operating pressure, temperature, current density, etc.) on pressure drop characteristics and it was concluded that the dominant factor is the anode side inlet flow rate. The parallel channel section of the flow bed design (Figure 1)

is responsible for the larger part of the calculated pressure losses. This model is used here to assess the effect of channel geometry on the overall cell hydraulic behaviour.

Figure 2 shows the effect of increasing the flow bed depth, in the range 0.5–4.0 mm, on the anode side pressure loss as a function of the inlet flow rate, for a constant channel width of 2 mm. Other conditions are: cell size 272 cm^2, current density 100 mA cm^{-2}, inlet temperature 80 °C, temperature gradient between inlet and outlet port 1 °C. For very shallow channels (less than 1.5 mm depth), as the channel depth decreases, the pressure drop rises rapidly. Above a depth of 2.0 mm there is not a significant reduction in pressure. The flow rate of methanol solution has a major effect on pressure drop at small channel depths but is not significant above depths of approximately 2 mm. In the DMFC efficient and rapid removal of carbon dioxide from the MEA is important for good cell electrical performance [40, 41]. Deep channels, and/or, high liquid velocity can generally enhance gas removal from the cloth surface (where it hinders reactant's supply to the reaction sites) by reducing the gas voidage in the two-phase mixture. Figure 2(a) indicates that a channel depth of 2.0 mm offers a reasonable compromise between low-pressure drop, effective gas release and material and machining costs of the bipolar plates.

Figure 2(b) shows the effect of increasing channel width, in the range 0.5–4.0 mm, as a function of anode side inlet flow rate on the total anode side pressure drop, for a constant flow bed depth of 2 mm. Other conditions are the same as in Figure 2(a). As expected increasing the width of the channel also reduces the total anode side pressure drop. Channel widths below 1 mm can result in significant pressure loss whilst channel widths above 2.5 mm do not result in significant reduction in pressure drop, at a constant flow rate. However, by increasing the channel width the number of the channels present in the flow bed, and thus the number of ribs that provide support to the MEA, are reduced. In addition with increasing channel width, above approximately 3 mm, the current distribution over the MEA becomes less uniform [43]. Overall a compromise between all the above requirements indicates that a channel width of 1.5 to 2.5 mm is a sensible choice.

Figure 3 shows a comparison of the pressure drop measured for a three cell stack with model predictions for single phase methanol solution flow. The experimental data and model predictions are in reasonable agreement and, although the simulation model is, in general, concerned about two phase flow, thus confirms that the model is suitable for the purpose of stack hydraulic performance prediction.

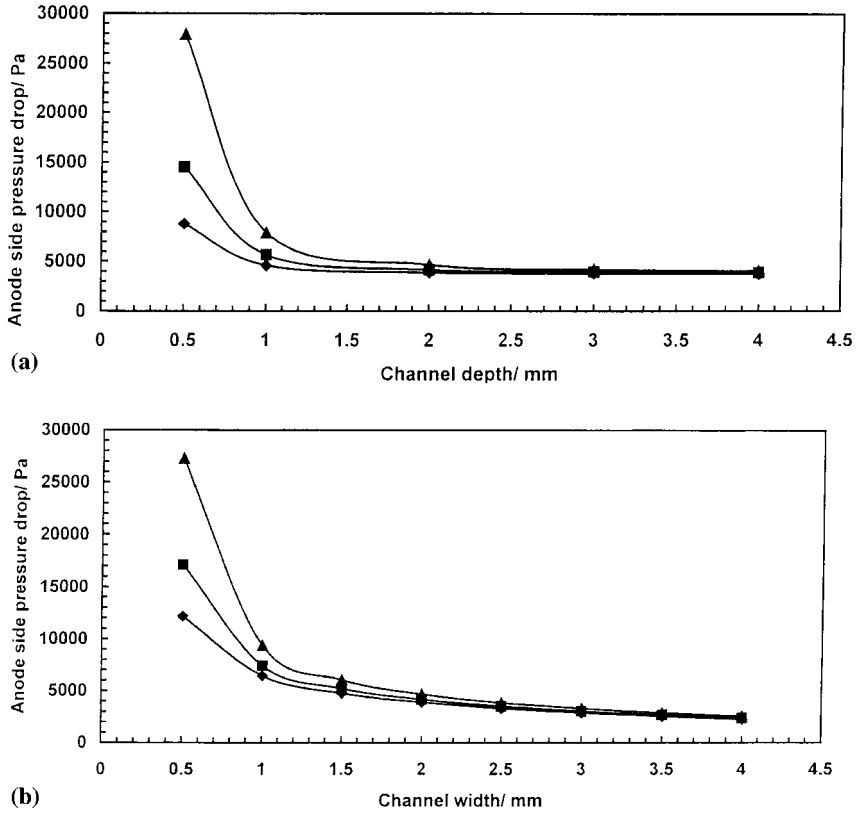

Fig. 2. The effect of increasing the channel depth and channel width on the pressure drop (cell size 272 cm^2, current density 100 mA cm^{-2}, inlet temperature 80 °C, temperature gradient between inlet and outlet port 1 °C). (a) The effect of increasing the channel depth in the range 0.5–4.0 mm as a function of anode side inlet flow rate and for a constant channel width of 2 mm. (b) Total anode side pressure drop for increasing channel width in the range 0.5–4.0 mm as a function of anode side inlet flow rate and for a constant channel depth of 2 mm. Key for (a) and (b): (◆) 0.5, (■) 1.0 and (▲) 2.0 dm^{-3} min^{-1}.

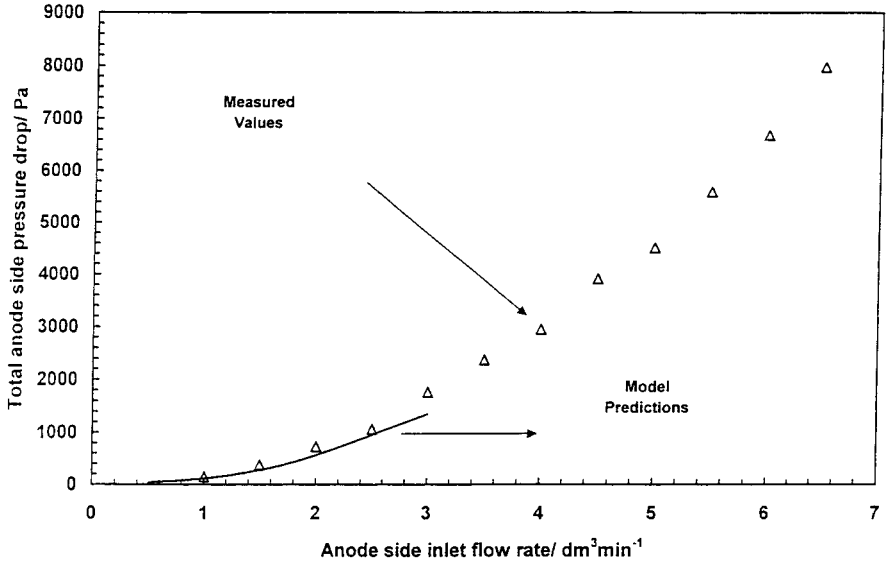

Fig. 3. Total anode side pressure drop for increasing channel width in the range 0.5–4.0 mm as a function of anode side inlet flow rate and for a constant channel depth of 2 mm (cell size 272 cm^2, current density 100 A cm^{-2}, inlet temperature 80 °C, temperature gradient between inlet and outlet port 1 °C).

The data of Figure 2, and the arguments above, suggest that a 2 mm × 2 mm cross section is a suitable dimension for the flow channel in the DMFC. Figure 4 shows the effect of varying the square cross section of the flow channel on the pressure drop in the range 1–16 mm^2, as a function of anode side inlet flow rate. The data is similar to that in Figure 2, for the case of the increasing channel width, and confirms that, for the specific flow bed design, a square channel with dimensions of either 2.0 mm × 2.0 mm or 2.5 mm × 2.5 mm is suitable in terms of hydraulic behaviour.

3.2. *Reverse type manifold*

Good electrical performance of a DMFC cell requires relatively high methanol solution flow rates [8, 40–42]: which provides improved heat and mass transfer characteristics of the cell, reduction, or elimination, of dead flow areas, and fast carbon dioxide removal. It is therefore important to have a uniform flow distribution in a fuel cell stack to avoid variations in electrical performance of cells and also to avoid overheating from insufficient heat removal from the stack. The distribution of flow in a fuel cell will depend upon the adopted manifold design. There are a number of different manifold designs, which can be considered for the DMFC, as shown in Figure 1B. However for hydraulic connection to a DMFC the problems of connection of large flow ports to the edge of bipolar plates generally restricts the choice of manifold design to either the reverse flow or parallel flow design. The reverse flow design offers the attraction of enabling the stack cell

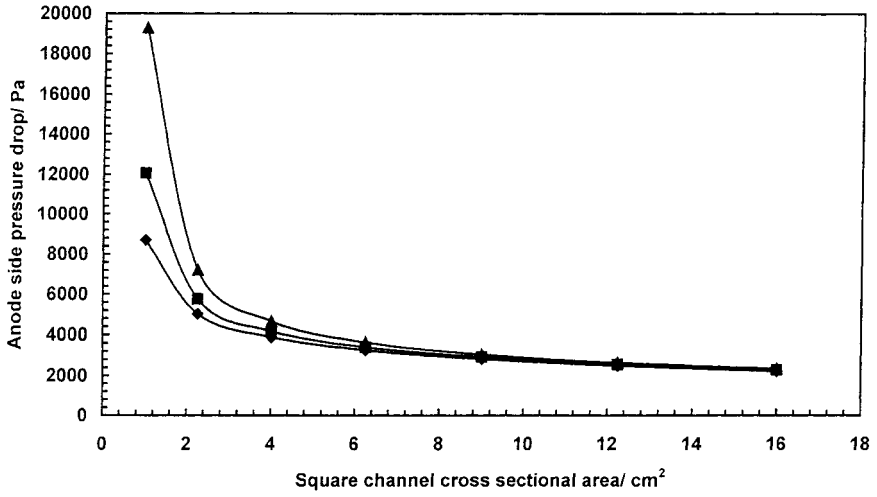

Fig. 4. The effect of keeping the channel cross section square and altering both its dimensions in the range 0.5–4.0 mm as a function of anode side inlet flow rate (cell size 272 cm^2, current density 100 A cm^{-2}, inlet temperature 80 °C, temperature gradient between inlet and outlet port 1 °C). Key: (◆) 0.5, (■) 1.0 and (▲) 2.0 dm^{-3} min^{-1}.

number to be varied without disturbing the ancillary pipe work and equipment connected to the cell stack. This is particularly important in prototype stack studies at the pilot scale.

We have developed a flow model, based on the model for single cell pressure drop behaviour, for a reverse flow manifold based DMFC stack system [24]. Two dominant factors identified from the model, for a stack of fixed internal manifold size, which determine the flow distribution are the individual cell anode side pressure drop and the high hydraulic resistances in the inlet and outlet port. These two factors produce significant, if not severe, flow maldistributions especially for a large number of stacked cells. In the preceding section we have investigated the effect of channel size on individual cell pressure drop performance. We thus consider here the effect of the channel dimension and also the internal manifold flow port cross sectional area on flow distribution in the reverse flow manifold design. The range of channel depth is dictated by practical thickness of the graphite block in use for the DMFC and requirements of relatively low pressure drop and hence we consider the range of 0.5–4.0 mm.

Figure 5 presents flow distribution behaviour, that is, the inlet volumetric flow rate of methanol solution to each cell, for a small stack of five cells, as a function of flow bed depth. The conditions of operation are: Anode side inlet flow rate $5.0\,dm^3\,min^{-1}$, current density 100 mA cm^{-2}, inlet temperature of 80 °C, temperature gradient between inlet and outlet port 1 °C, inlet manifold diameter 15.0 mm, outlet manifold diameter 25.0 mm. As shown in Figure 5, there is a significant variation in flow rate between the cells. For a flow bed depth less than 1.0 mm the variation in flow rate, around the ideal value of $1.0\,dm^3\,min^{-1}$ for each cell, is as high as ±40%, with higher flows in the cells closer to the inlet and exit to the cell stack. As the depth increases, the flow distribution becomes more uniform and for the case of 3.0 mm bed depth an almost uniform flow distribution is achieved, with only the last cell having a relatively low flow rate. In the case of the 4.0 mm channel depth the flow distribution reverses and is now greater in the cells further away from the point of flow entry into the cell stack. The variation in flow rate is in the range of ±15%, which for larger stacks will potentially create a more serious flow maldistribution problem.

To explain the flow variation behaviour of the stack it should be remembered that the channel depth significantly affects pressure drop behaviour of the single cell (Figure 2). We know that for the cell stack, in general, all the flow paths (i.e., fluid streams between inlet port-of cell *i*- and its outlet port) should result in equal pressure drops. For cells with small channel dimensions the friction losses in the manifolds are small in comparison with those inside the flow bed. Hence to satisfy the equality of pressure in all flow paths a higher quantity of fluid passes through the first cells. As the flow bed becomes deeper, than 2 mm, the pressure losses inside the cells reduce rapidly and become comparable with the pressure losses in the manifolds. In that case the characteristics of the two phase flow and manifold fluid mechanics, as discussed in Section 2.1, lead to a reverse of the flow distribution pattern. Overall it appears that the optimal flow bed depth for the stack under investigation is of the order of 3.0 ± 0.5 mm.

The other factor, which can influence the flow distribution, is the manifold cross section area. For a large DMFC stack, (e.g., with an active cell cross section

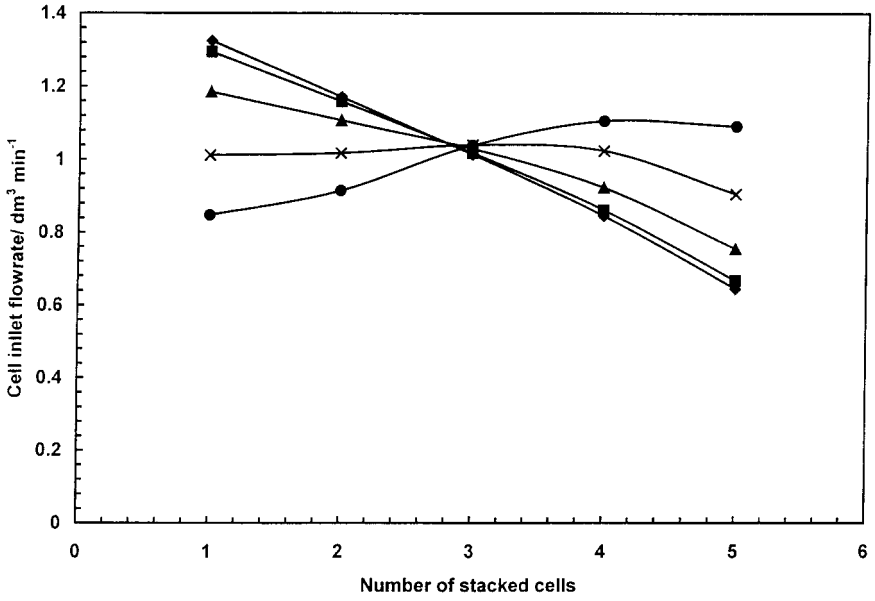

Fig. 5. Flow distribution patterns for a five-cell stack as a function of flow bed depth (anode side inlet flow rate 5.0 $dm^3\,min^{-1}$, current density 100 mA cm^{-2}, inlet temperature of 80 °C, temperature gradient between inlet and outlet port 1 °C, inlet manifold diameter 15.0 mm, outlet manifold diameter 25.0 mm). Key: (◆) 0.5, (■) 1.0, (▲) 2.0, (×) 3.0 and (●) 4.0 mm.

area of 270 cm^2 and stack cross sectional area 625 cm^2, as developed at Newcastle) the practical manifold internal size range is between 10.0 to 30.0 mm diameter. Figure 6 shows the flow distribution patterns in a 10 cell DMFC stack for a variety of inlet to outlet manifold diameter ratios. The operating conditions are: anode side inlet flow rate 10.0 $dm^3\,min^{-1}$, current density 100 mA cm^{-2}, inlet temperature 80 °C, temperature gradient between inlet and outlet port 1 °C. In general, we can state that the dividing (inlet) manifold diameter is the most critical one in determining the flow distribution and that the combining (outlet) manifold diameter should be bigger that the inlet. It is evident that the smaller the inlet manifold diameter the poorer is the flow distribution with, under certain conditions, the flow to the two cells close to the inlet significantly lower than the remaining cells. Thus these first cell to the stack may be underfed with methanol solution. As the manifold diameter increases, then gradually the flow to the cells close to the inlet ports increases and eventually exceeds the design requirement of 1.0 $dm^3\,min^{-1}$. An inlet manifold diameter of approximately 15.0 mm, in combination with an outlet diameter of 25 mm, appears to give the better flow distribution, under the conditions considered here.

Overall we have shown that altering the flow bed depth and/or the dividing manifold diameter can greatly affect the flow distribution in a multicell DMFC stack. For a specific stack design, and for a fixed number of stacked cells, the model can determine the flow bed depth and the manifold dimensions to achieve an 'optimum' hydraulic behaviour. Nevertheless it is evident from the model that the reverse flow manifold configuration, despite any improvements realised from an optimised design, is far from satisfactory for the DMFC stack. Hence, alternative manifold design configurations should be evaluated with the aid of modelling; one such configuration is a parallel design manifold.

3.3. *Parallel vs reverse type manifold*

Figure 1B(a) shows the parallel manifold configuration schematically. As reported above the flow distribution with the reverse type manifold is far from being ideal with severe flow nonuniformity possible, especially for stacks with a large number of cells. Figures 7 and 8 show the flow distribution in identical DMFC stacks, operating under the same conditions (theoretical *i*th cell inlet flow rate 1.0 $dm^3\,min^{-1}$, current density 100 mA cm^{-2}, inlet temperature 80 °C, temperature gradient between inlet and outlet port 1 °C), with the two manifold configurations. It is evident that the parallel configuration manifold gives a superior flow distribution. For example, with the parallel flow manifold the flow variation for a 16-cell stack is ±10%, while for the reverse flow manifold configuration the flow variation is ±80%. These results were based on the assumption that we attempt to feed each cell with the same flow rate of 1.0 $dm^3\,min^{-1}$of methanol solution. The flow distribution is a critical factor because it determines the efficiency of carbon dioxide removal, the flow pattern inside the flow bed, the overall stack heat management, and most significantly the electrical performance. As can be seen from Figure 7, for the reverse flow manifold there are severe flow maldistribution

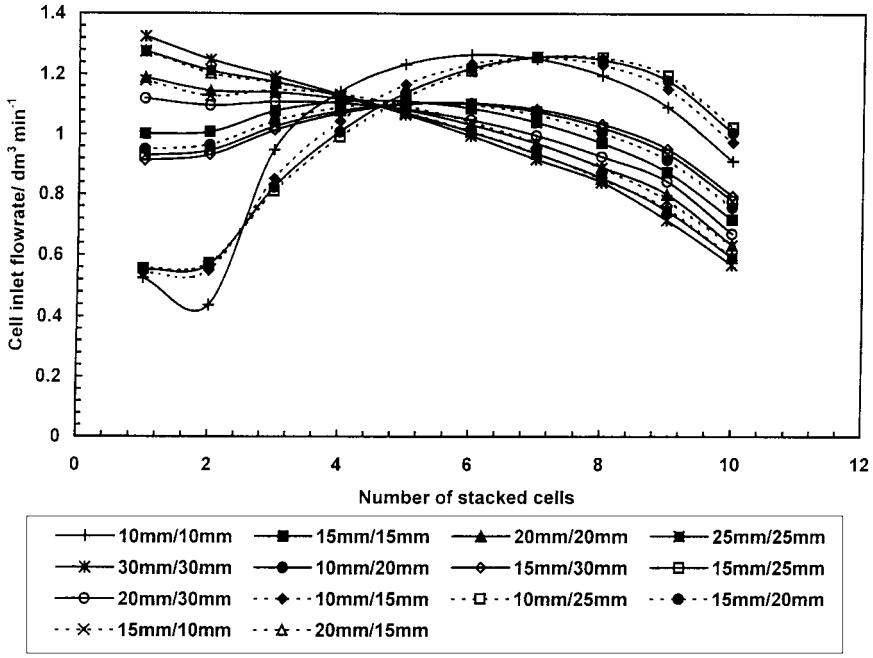

Fig. 6. Flow distribution pattern for a 10 cell stack with a reverse manifold configuration for different port diameters. Anode side inlet flow rate 1.0 $dm^3\,min^{-1}$/cell, current density 100 mA cm^{-2}, inlet temperature 80 °C, temperature gradient between inlet and outlet port 1 °C. (ratio of inlet to outlet manifold diameters shown on figure).

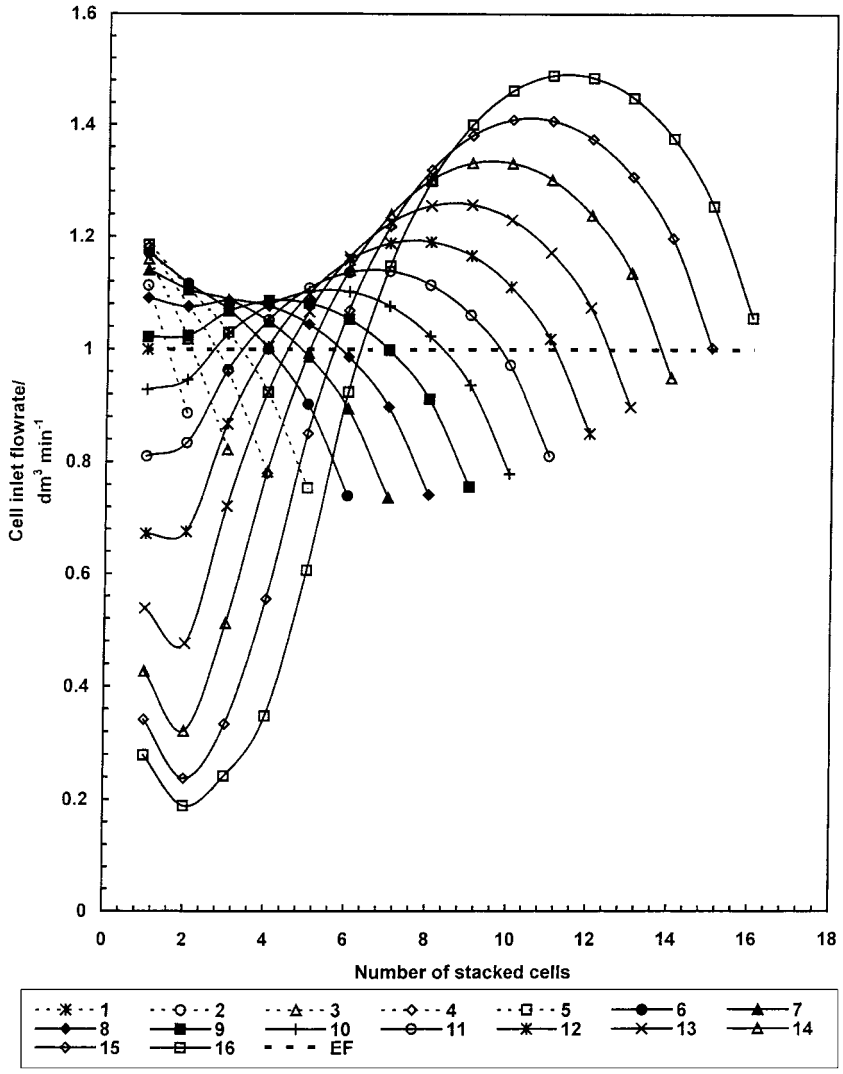

Fig. 7. Flow distribution pattern for a multicell stack with a reverse manifold configuration. Anode side inlet flow rate 1.0 $dm^3\ min^{-1}$/cell, current density 100 mA cm^{-2}, inlet temperature 80 °C, temperature gradient between inlet and outlet port 1 °C, 2 mm by 2 mm channel dimensions, 15.0 mm inlet manifold diameter, 25 mm outlet manifold diameter.

problems, especially when the number of cells in the stack exceeds 10. When there are less than 10 cells in the stack all the cells receive an inlet flow rate in the range of $1.0 \pm 0.2\,dm^3\,min^{-1}$, instead of the required $1.0\,dm^3\,min^{-1}$. This range is considered as acceptable in terms of electrochemical performance and from stack thermal management point of view. For more than 10 cells the situation deteriorates rapidly, for example, for a 16-cell stack the first cell is fed with only $0.2\,dm^3\,min^{-1}$ of methanol solution. This could result in several potential problems in stack operation. One of these is the available concentration of methanol in individual cells under high current load. With a low solution flow rate, and a thus a high residence time, high conversions of methanol may be achieved which will cause a significant reduction in methanol concentration and thus cause a significant fall in individual cell voltage and thus power output. This is in addition to problems of managing large amounts of carbon dioxide gas generation as discussed below.

Figures 9 and 10 show the flow distribution patterns for 10-cell stacks with the reverse flow manifold and with the parallel manifold, for increasing anode side liquid flow rate. The operating conditions are: current density 100 mA cm^{-2}, inlet temperature 80 °C, temperature gradient between inlet and outlet port 1 °C. Again it is evident that the parallel manifold generally produces a better flow distribution, than the reverse flow manifold, over a wide range of liquid phase flow rates. Even with high flow rates (of the order of 1.5–2.0 $dm^3\,min^{-1}$ per cell) the variation in individual cell inlet flow rate is small with the exception of the last cell, which is slightly underfed (but still is at an acceptable level). In the case of the reverse flow manifold (Figure 9), the flow is not well distributed over almost the whole range of flow rates under investigation (3–20 $dm^3\,min^{-1}$). At low flow rates the distribution in flow is not uniform, varying by approximately ±45% around the design values. As the overall flow rate is increased the flow becomes more uniform, but on

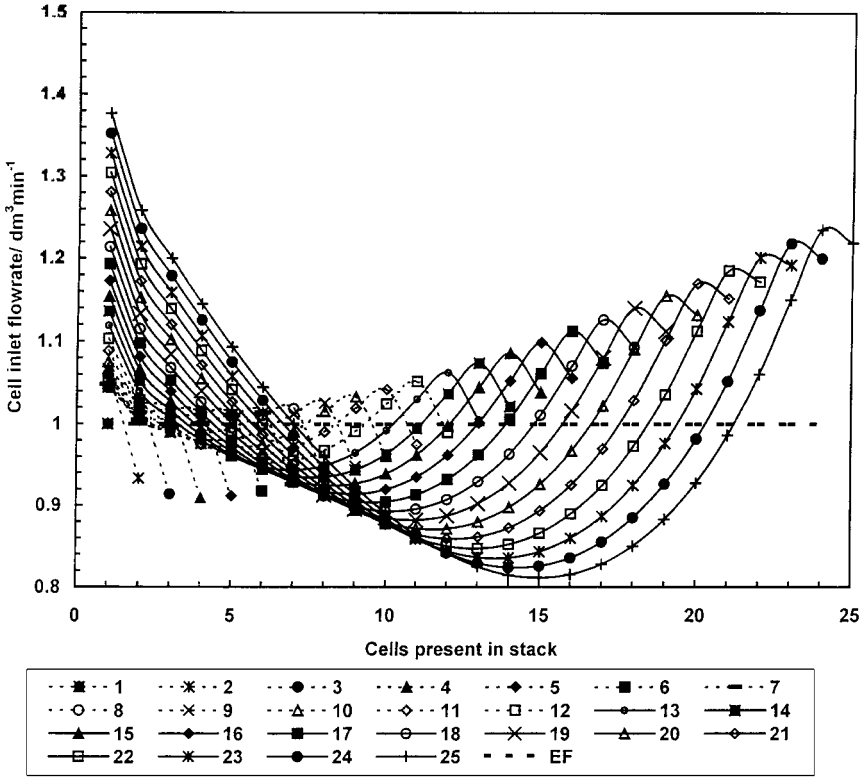

Fig. 8. Flow distribution pattern for a multicell stack with a parallel manifold configuration. Anode side inlet flow rate 1.0 dm^3 min^{-1}/cell, current density 100 mA cm^{-2}, inlet temperature 80 °C, temperature gradient between inlet and outlet port 1 °C, 2 mm by 2 mm channel dimensions, 15.0 mm inlet manifold diameter, 25 mm outlet manifold diameter.

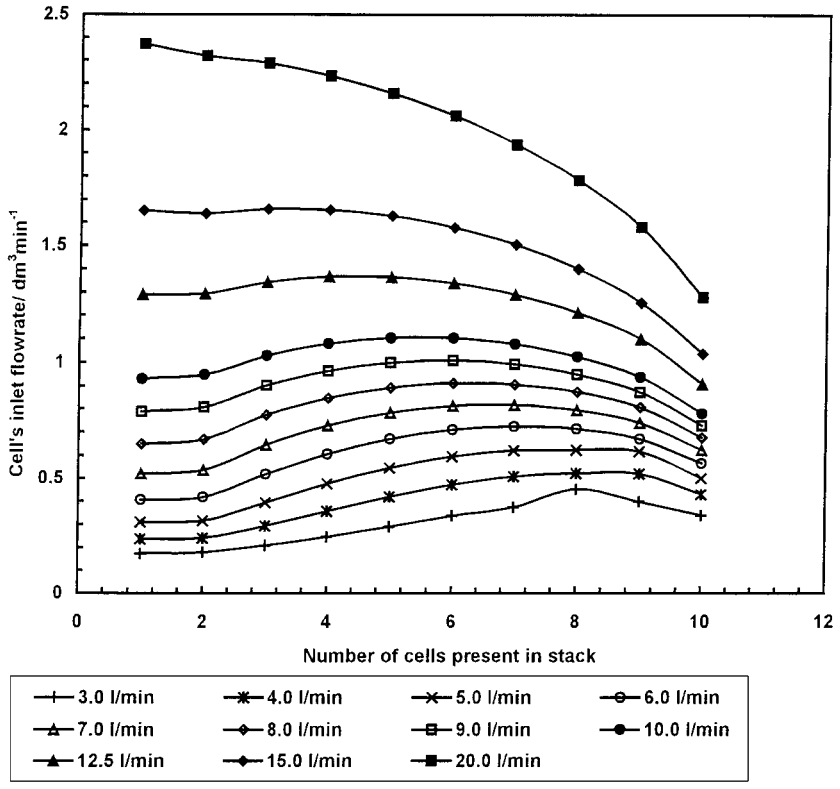

Fig. 9. Flow distribution pattern for a 10-cell stack with a reverse manifold configuration as a function of increasing anode side liquid phase inlet flow rate. Current density 100 mA cm^{-2}, inlet temperature 80 °C, temperature gradient between inlet and outlet port 1 °C, 2 mm by 2 mm channel dimensions, 15.0 mm inlet manifold diameter, 25 mm outlet manifold diameter.

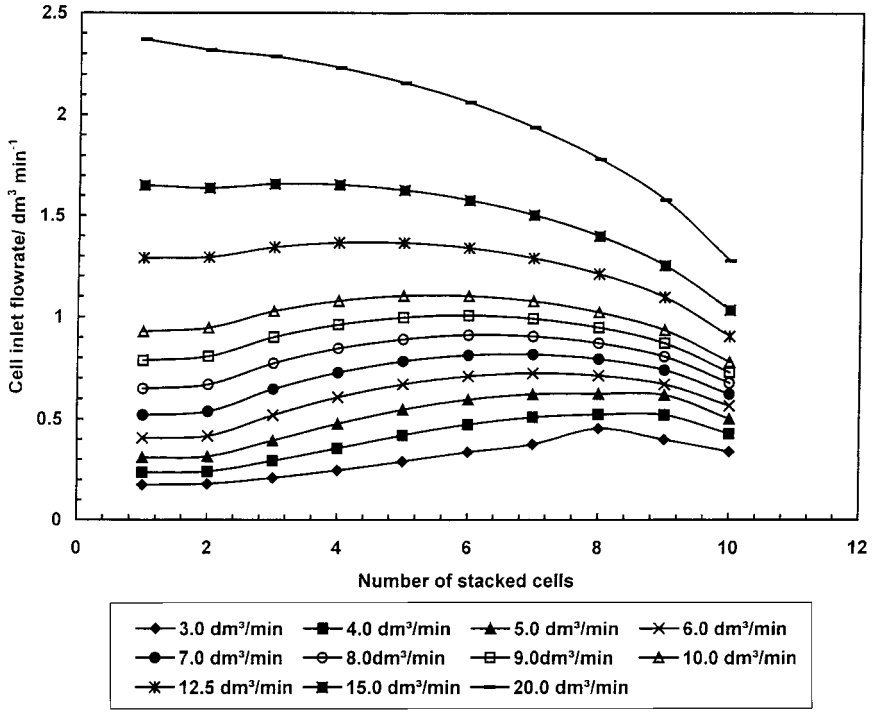

Fig. 10. Flow distribution pattern for a 10-cell stack with a parallel manifold configuration as a function of increasing anode side liquid phase inlet flow rate. Current density 100 mA cm^{-2}, inlet temperature 80 °C, temperature gradient between inlet and outlet port 1 °C, 2 mm by 2 mm channel dimensions, 15.0 mm inlet manifold diameter, 25 mm outlet manifold diameter.

increasing flow rate, above say 9 $dm^3\,min^{-1}$ the flow distribution deteriorates, and leads to serious flow maldistributions (with large variations of 1.0 $dm^3\,min^{-1}$ between the first and the last cell of the stack).

Figure 11 shows the effect of current density on the model predictions of the anode side flow distribution for a three-cell stack with a reverse flow manifold. The operating conditions are: inlet temperature 80 °C, anode side inlet flow rate 1.5 $dm^3\,min^{-1}$, temperature gradient between inlet and outlet port 1 °C. As can be seen from the figure with low to medium range current densities (i.e., <200 mA cm^{-2}) the role of the increased carbon dioxide (which changes the quality of the two phase flow mixture) production is diminished. At the higher current density investigated here there is a noticeable effect on anode side flow distribution due to the significant volume change of the system (31% increase), the flow varies by ±14% around the average value. With an increase in current density and in the number of cells in the stack the distribution of flow to the cells becomes wider.

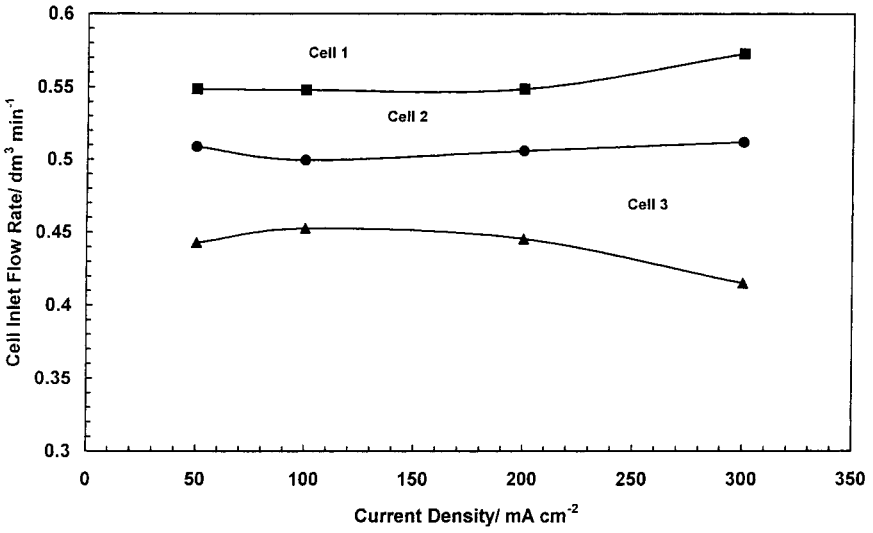

Fig. 11. Flow distribution pattern for a three-cell stack with a reverse manifold configuration as a function of increasing applied current density. Anode side inlet flow rate 1.5 $dm^3\,min^{-1}$, inlet temperature 80 °C, temperature gradient between inlet and outlet port 1 °C, 2 mm by 2 mm channel dimensions, 15.0 mm inlet manifold diameter, 25 mm outlet manifold diameter.

3.4. *Stack pressure drop*

A further factor in stack design is the total pressure drop requirements for the stack, as this dictates power consumption for pumping and hence affects the overall system net power performance. Figure 12 compares the pressure drop experienced with the two manifold configurations for an increasing number of stacked cells. Overall the variation in pressure drop between the two manifold arrangements is small with the parallel design giving a 2–20% lower pressure drop. Figure 13 compares the pressure drops for both manifold designs, with a 10-cell DMFC stack, as a function of increasing inlet flow rate. For low flow rates the reverse flow manifold gives lower pressure drop performance. As the flow is increased there is a transition point near 15.0 $dm^3 min^{-1}$ where the parallel design produces the lowest pressure drop. The differences in the total anode side pressure drop, however, are always less than $\pm 10\%$, and do not indicate any superiority of either design in terms of pressure drop behaviour.

4. Conclusions

We have used mathematical models to investigate the flow pressure drop behaviour in the anode side of direct methanol fuel cell anodes. The effect of a change in the dimensions of the flow channels in the flow bed on the hydraulic behaviour of the cell was investigated. It was found that for small widths/depths the pressure losses are quite significant but decrease quickly on enlarging the channel dimension. The model indicates that a square channel with dimensions between 2–2.5 mm gives a suitable performance when practical issues and cost of bipolar plate design are considered.

We have used mathematical models to investigate the flow distribution in DMFC stack with two different

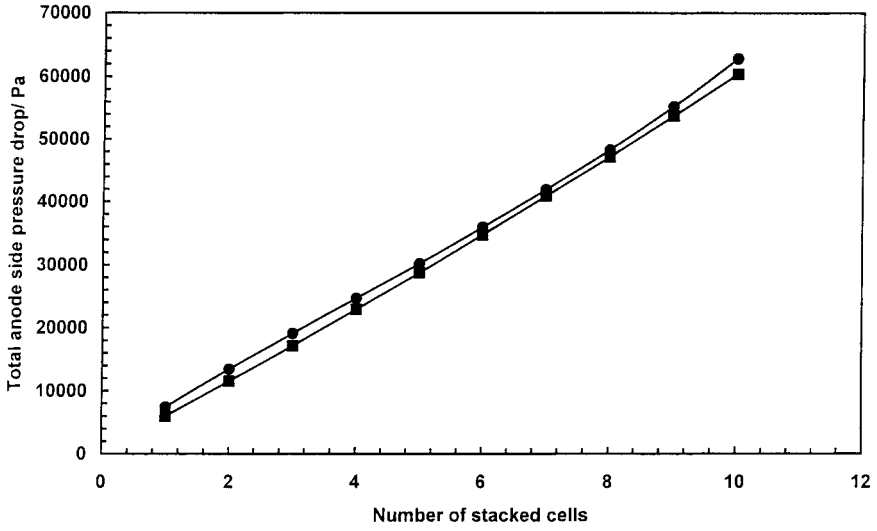

Fig. 12. Comparison of the two manifold designs in terms of overall anode side pressure drop as a function of increasing number of stacked cells. Anode side inlet flow rate 1.0 $dm^3 min^{-1}$/cell, current density 100 mA cm^{-2}, inlet temperature 80 °C, temperature gradient between inlet and outlet port 1 °C, 2 mm by 2 mm channel dimensions, 15.0 mm inlet manifold diameter, 25 mm outlet manifold diameter. Key: (●) reverse type manifold and (■) parallel type manifold.

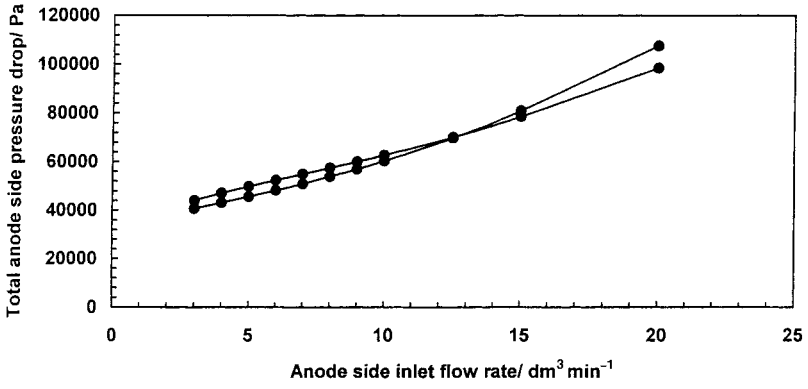

Fig. 13. Comparison of the two manifold designs in terms of overall anode side pressure drop as a function of increasing anode side liquid phase inlet flow rate. 10 cell, stack, current density 100 mA cm^{-2}, inlet temperature 80 °C, temperature gradient between inlet and outlet port 1 °C, 2 mm by 2 mm channel dimensions, 15.0 mm inlet manifold diameter, 25 mm outlet manifold diameter. Key: (●) reverse type manifold and (■) parallel type manifold.

manifold designs; reverse flow and parallel flow. Two methods of improving the flow distribution pattern produced by the reverse manifold configuration were examined: deepening the flow depth and altering the manifold diameter. Both methods could alleviate the flow maldistribution but nevertheless, for large scale practical stacks, the existing design is far from suitable and may lead to problems in operation if low flow rates are used. A preliminary assessment of a parallel flow manifold design demonstrated its superiority in terms of uniform flow distribution, especially in the case of large stacks. In terms of pressure drop behaviour no clear advantage was found for either design.

Acknowledgements

The authors would like to acknowledge the European Commission for supporting P. Argyropoulos under a B20 TMR Marie Curie research–training grant, and EPSRC for supporting Dr W.M. Taama.

References

1. X. Ren, M.S. Wilson and S. Gottesfeld, *J. Electrochem. Soc.* **143** (1996) L12–L15.
2. V.M. Schmidt, P. Brockerhoff, B. Hohlein, R. Menzer and U. Stimming, *J. Power Sources* **49** (1994) 299.
3. S.R. Narayanan, G. Halpert, W. Chun, B. Jeffries-Nakamura, T.I. Valdez, H. Frank and S. Surampudi, *in* 37th Power Sources Conference, Cherry Hill, NJ (1996).
4. S.R. Narayanan, G. Halpert, W. Chun, B. Jeffries-Nakamura, T.I. Valdez, H. Frank and S. Surampudi, *in* Electrochemical Society Annual Meeting, Los Angeles, CA (1996).
5. S.R. Narayanan, T.I. Valdez, N. Rohatgi, W. Chun and G. Halpert, *in* Fuel Cell Seminar, Palm Springs, CA (1998).
6. X. Ren, S.C. Thomas, P. Zelenay and S. Gottesfeld, *in* 1998 Fuel Cell Seminar, Palm Springs, CA (1998).
7. K. Scott, W.M. Taama and P. Argyropoulos, *J. Appl. Electrochem.* **28** (1999) 1389.
8. K. Scott, W.M. Taama and P. Argyropoulos, *J. Power Sources* **79** (1999) 43.
9. A.K. Shukla, M.K. Ravikumar, M. Neergat and K.S. Gandhi, *J. Appl. Electrochem.* **29** (1999) 129.
10. A.K. Shukla, P.A. Christensen, A.J. Dickinson and A. Hamnett, *J. Power Sources* **76** (1998) 54.
11. D.H. Jung, C.H. Lee, C.S. Kim and D.R. Shin, *J. Power Sources* **71** (1998) 169.
12. D.H. Jung, C.H. Lee, C.S. Kim and D.R. Shin, *J. Power Sources* **71** (1998) 174.
13. D.H. Jung, C.H. Lee, Y. Chun and D. Peck, *in* 1998 Fuel Cell Seminar, Palm Springs, CA (1998).
14. M.K. Ravikumar, PhD thesis, Indian Institute of Science (1996).
15. A.S. Arico, P. Creti, N. Giordano, V. Antonucci, P.L. Antonucci and A. Chuvilin, *J. Appl. Electrochem.* **26** (1996) 959.
16. J. Cruickshank and K. Scott, *J. Power Sources* **70** (1998) 40.
17. M.K. Ravikumar and A.K. Shukla, *J. Electrochem. Soc.* **143** (1996) 2601.
18. J.T. Wang, J.S. Wainright, R.F. Savinell and M. Litt, *J. Appl. Electrochem.* **26** (1996) 751.
19. S. Wasmus and W. Vielstich, *J. Appl. Electrochem.* **23** (1993) 120–124.
20. P. Argyropoulos, K. Scott and W.M. Taama, *Chem. Eng. J.* **73** (1999) 217.
21. P. Argyropoulos, K. Scott and W.M. Taama, *Chem. Eng. J.* **73** (1999) 229.
22. P. Argyropoulos, K. Scott and W.M. Taama, *J. Power Sources* **79** (1999) 169.
23. P. Argyropoulos, K. Scott and W.M. Taama, *J. Power Sources* **79** (1999) 184.
24. P. Argyropoulos, K. Scott and W.M. Taama. Submitted to *J. Fluid Eng.*
25. J.B. Riggs, *Indust. & Eng. Chem. Res.* **26** (1987) 129.
26. R.A. Bajura and E.H. Jones, *J. Fluid Eng.* (Dec. 1976) 654.
27. A. Acrivos, B.D. Babcock and R.L. Pigford, *Chem. Eng. Science* **10** (1959) 112.
28. R.A. Bajura, *J. Eng. Power* (Jan. 1971) 7–12.
29. A.B. Datta and A.K. Majumdar, *Int. J. Heat & Fluid Flow* **2** (1980) 253.
30. A.K. Majumdar, *Appl. Math. Model.* **4** (1980) 424.
31. X. Ren, W. Henderson and S. Gottesfeld, *J. Electrochem. Soc.* **144** (1997) L267.
32. D. Weng, J.S. Wainright, U. Landau and R.F. Savinell, *J. Electrochem. Soc.* **143** (1996) 1260.
33. T.A. Zawodzinski, J. Davey, J. Valerio and S. Gottesfeld, *Electrochim. Acta* **40** (1995) 297.
34. A. Kuver and W. Vielstich, *J. Power Sources* **74** (1998) 211.
35. R.J. Boersma and N.M. Sammes, *J. Power Sources* **66** (1997) 41.
36. W. Beitz and K. Kuttner, *in* M. Shields (ed.), 'Dubbel: Handbook of Mechanical Engineering', (Springer-Verlag, 1994).
37. V.D. Inginieure, 'VDI Warme-Atlas: Berechnungsblatter fur den Warmeubergang'. (Verein Deutscher Inginieure, Dusseldorf, 1991).
38. S.M. Walas, *in* H. Brenner (ed.) 'Chemical Process Equipment: Selection and Design', (Butterworth-Heinemann Series in Chemical Engineering, Boston, 1990).
39. A.C. West and T.F. Fuller, *J. Appl. Electrochem.* **26** (1996) 557.
40. P. Argyropoulos, K. Scott and W.M. Taama, *Electrochim. Acta* **44** (1999) 3575.
41. P. Argyropoulos, K. Scott and W.M. Taama, *J. Appl. Electrochem.* **29** (1999) 661.
42. K. Scott, P. Argyropoulos, S. Kraemer, K. Sundmacher and W.M. Taama, *in* 1998 Fuel Cell Seminar, Palm Springs, CA (1998).
43. K. Scott, *J. Appl. Electrochem.* (in preparation).
44. F.P. Incropera and D.P. DeWitt, 'Introduction to Heat Transfer'. 3rd edn (J. Wiley & Sons, New York, 1996).